JACS
JOURNAL OF THE AMERICAN CHEMICAL SOCIETY
Article
pubs.acs.org/JACS

# Improving Stability of Zeolites in Aqueous Phase via Selective Removal of Structural Defects

Sebastian Prodinger,[†] Miroslaw A. Derewinski,[*,†] Aleksei Vjunov,[†] Sarah D. Burton,[†] Ilke Arslan,[†] and Johannes A. Lercher[*,†,‡]

[†]Institute for Integrated Catalysis, Pacific Northwest National Laboratory, P.O. Box 999, Richland, Washington 99352, United States
[‡]Department of Chemistry and Catalysis Research Institute, TU München, Lichtenbergstrasse 4, 85748 Garching, Germany

Supporting Information

**ABSTRACT:** Missing silicon−oxygen bonds in zeolites are shown to be the cause for structural instability of zeolites in hot liquid water. Their selective removal drastically improved their structural stability as demonstrated using zeolite beta as example. The defects in the siloxy bonds were capped by reaction with trimethylchlorosilane, and Si−O−Si bonds were eventually formed. Hydrolysis of Si−O−Si bonds of the parent materials and dissolution of silica−oxygen tetrahedra in water causing a decrease in sorption capacity by reprecipitation of dissolved silica and pore blocking was largely mitigated by the treatment. The stability of the modified molecular sieves was monitored by $^{29}$Si-MAS NMR, transmission electron micrographs, X-ray diffraction, and adsorption isotherms. The microporosity, sorption capacity, and long-range order of the stabilized material were fully retained even after prolonged exposure to hot liquid water.

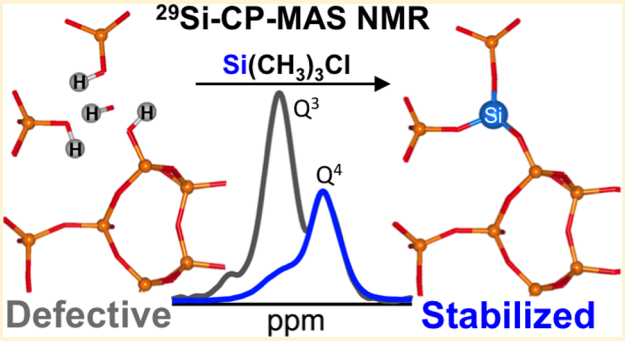


## INTRODUCTION

Porous aluminosilicates such as zeolites are used as shape selective solid acid catalysts for many industrial processes.[1−3] While the stability against water in gas phase reactions has been studied extensively, much less is known about the chemistry of such materials in hot liquid water. Structural and functional stability are, however, essential to be able to use them as catalysts for reactions in which the presence of large concentrations of water is unavoidable. Recent work demonstrate the corrosive properties of hot liquid water and the rapid degradation of zeolites.[4]

Understanding the process of framework decay, as well as its prevention, has been addressed in several reports. We have recently shown the pathway of framework destruction in hot liquid water, starting with the selective hydrolysis of tetrahedrally coordinated Si (Si T-sites), and leading eventually to the dissolution and reprecipitation of silica. These processes are accompanied by a loss in sorption capacity and crystallinity.[5] At the same time, dealumination is not observed with the coordination of Al T-sites remaining mostly unchanged by treatment in hot liquid water.[6] The reduced catalytic activity is attributed to site blockage by reprecipitation of dissolved silica. The group of Resasco recently communicated an in-depth study of factors influencing the (poor) stability of zeolites in hot liquid water, confirming that the concentration of silanol defects and the hydrolysis of Si−O−Si bonds are the key factors in the lattice disintegration.[7]

It has been shown by the group of Resasco that hydrophobization with organosilanes improves framework stability of zeolite HY.[8,9] The initial method aims to lower the rates of hydrolysis by minimizing water concentration in the pores via silylation of the external surface.[8] Obviously, the approach may be limited if water is formed at high rates in the pores. Under such circumstances, only the direct prevention of the hydrolytic attack of water onto Si−O−Si bonds may stabilize the zeolite, a hypothesis postulated in the follow-up work by Zapata et al.[9]

On the basis of the detailed insight into the deconstruction of zeolite frameworks in hot liquid water, we decided to explore whether internal SiOH groups can be chemically healed or protected via reaction with a silylating agent. This approach has been explored previously,[10−13] to modify the chemical composition, as well as the acid and structural properties of zeolites. Chlorosilanes were used, for example, by Kraushaar et al., to characterize "SiOH nests", i.e., the group of up to four OH groups generated by removal of a tetrahedrally coordinated lattice cation.[12,13]

In this work, we explore the impact of reacting a silylating agent, trimethylchlorosilane (TMS-Cl), with a series of BEA zeolites with well-defined SiOH nest concentrations. The modified materials are examined for their hydrothermal stability and compared to the parent defect-rich zeolites. It will be shown that the stability in hot liquid water, as measured by the retention of the zeolite crystallinity, is improved for the silylated material. It will also be shown that, despite hydrolysis

**Received:** December 7, 2015
**Published:** March 13, 2016



DOI: 10.1021/jacs.5b12785
J. Am. Chem. Soc. 2016, 138, 4408−4415

generating mesopores in silylated and untreated materials, the microporosity is only retained in the stabilized material. This in turn implies that the specific size and shape selectivity in the BEA framework were also retained.

## RESULTS AND DISCUSSION

**Model System.** Three samples of zeolite beta (BEA) with varying concentration of defect sites synthesized from boron-containing materials were used to test the impact of improving framework stability through selective removal of structural defects. We focus on the BEA structure, because it has been previously used as an efficient catalyst for acid catalysis in water.[6] BEA has 12-membered ring pores organized in a three-dimensional network.[14,15] It occurs in three different polymorph structures, of which only polymorphs A (BEA) and B (BEB) are present in the investigated samples.

The intergrowth of the polymorphs, as well as their relative abundance, was assessed with X-ray diffraction (XRD). The X-ray diffractograms of the materials showed a variety of broad and sharp reflections as the result of the interplanar stacking faults. This disorder increases the tortuosity of the pores in the (001) plane.[16] Of the nine crystallographically distinct tetrahedral sites (T), Vjunov et al. recently showed that the Si $T_1$ and $T_2$ sites, connecting the 4-membered ring, are most accessible to hydrolysis.[5]

The boron containing BEA zeolites were synthesized by isomorphous substitution of the tetrahedral Si framework atoms with B.[17−19] Aluminum was present only in traces as a result of impurities in the silica source. Hence, the Si/Al ratio was higher than 150.

Water can leach boron from its framework position via nucleophilic attack, forming SiOH nests, i.e., four silanols within close vicinity and tetrahedral geometry. Generally, SiOH nests are considered to be labile at elevated temperatures, resulting in condensation of the hydroxyl groups, subsequent closure of SiOH nests, and a distortion of the framework structure.[20]

The zeolites were synthesized in the presence of $Na^+$ ions, to minimize charge compensation by the templating amines, which in turn would protect $B(SiO)_4^-$ units during calcination.[21] During the ion exchange step, $Na^+$ cations were replaced with $NH_4^+$, which were then decomposed in one last calcination step. Compared to $Na^+$ and $NH_4^+$, the resulting charge balancing protons are very poor in maintaining the tetrahedral coordination of the framework boron at high calcination temperatures.[22] As a result, it becomes trigonally bonded to the framework. In the final step, boron is completely removed from the framework as $BO_4^-$ in the presence of water[23] as verified by $^{11}$B-MAS NMR. The defect-form (e.g., $BEA14_{def}$) obtained in this way has defined concentrations of SiOH nests, which directly correlate to the Si/B ratios of the as-made material.

The physicochemical characterization data of the three B-BEA zeolites from which defect-rich materials were derived are shown in Table 1. An upper limit for the concentration of B incorporated corresponding to a Si/B ratio of 14 is apparent.

It appears that the maximum packing density of the charge balancing cations determines this upper concentration.[18,24]

The morphologies of the as-made zeolites were probed macroscopically with He ion microscopy (HIM) (Figure S1). All showed well-separated, large pillow-shaped particles ($d \sim 1$ $\mu$m) with terrace structures indicating growth along the $z$-axis.[25] The uniformity of the samples, independent of their Si/B ratio, was also reflected in the $N_2$-physisorption isotherms (Table 1), indicating nearly identical micro- and mesopore volumes for all three samples.

**Table 1. Elemental Analysis and $N_2$-Physisorption Data**

| sample | $Si/B_{as\ made}$ | B concentration [mmol/g][a] | micropore volume [$cm^3$/g] | mesopore volume [$cm^3$/g] |
|---|---|---|---|---|
| B-BEA14 | 14 | 0.88 | 0.23 | 0.05 |
| B-BEA16 | 16 | 0.81 | 0.23 | 0.03 |
| B-BEA19 | 19 | 0.67 | 0.25 | 0.08 |

[a]Elemental analysis is based on the calcined Na-form. $N_2$-physisorption data is based on defect form of the material.

Note that only B-BEA19 showed a hysteresis loop in the sorption isotherm (Figure S4), indicating some mesoporosity. The HIM images in Figure S1 indicate a larger presence of smaller particles for B-BEA19, which is concluded to induce mesopore formation between particles.

**Strategies to Remove Structural Defects via Si-Reincorporation.** A large number of silylating agents capable of reacting with SiOH groups has been documented in literature, including $SiCl_4$,[11] silanes $Si(CH_3)_xCl_{4-x}$,[10,12] octadecyltrichlorosilane[8] or hexamethydisilazane.[10] The approach of Kraushaar et al., who silylated silicalite with $Si(CH_3)_3Cl$ (TMS-Cl) was adopted for this study.[13,26] TMS-Cl was chosen to minimize the concentration of HCl formed during surface reactions. To scale production of stabilized zeolites, a flow reactor system was developed, in which silane vapors were passed through the reactor bed using $N_2$ as carrier gas. The typical reaction pathway for removal of SiOH nests is depicted in Scheme 1. In the first step, TMS-Cl caps a SiOH defect through a condensation reaction accompanied by the release of HCl. In subsequent steps, further defect healing is achieved by Si−O−Si bridge formation and methyl group removal, likely in the form of methane. The optimized reaction conditions are reported in Table S1 in the Supporting Information.

**Scheme 1. Schematic Depiction of the Stepwise Process of a Typical Silylation Procedure, Showing the Removal of Silanol Nests in BEA Structure, and the Associated $^{29}$Si Chemical Shifts, Is Shown[a]**

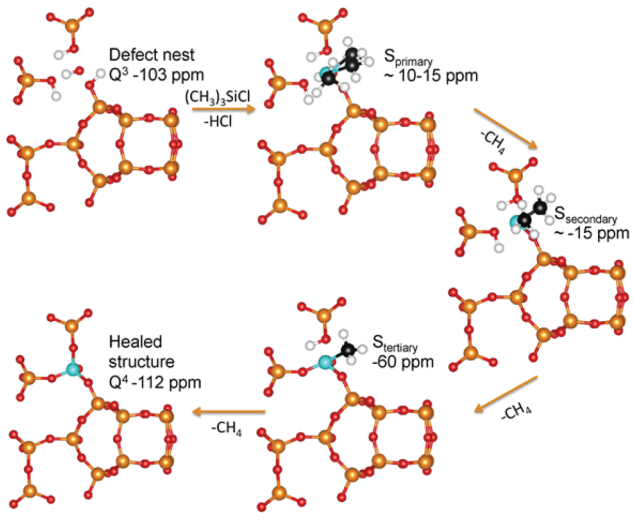


[a]Color coding is as follows: carbon, black; hydrogen, white; incorporated silicon, turquoise; framework silicon, orange; oxygen, red.



DOI: 10.1021/jacs.5b12785
J. Am. Chem. Soc. 2016, 138, 4408−4415

To test the thermal stability of silylated samples, thermogravimetric analysis coupled with a differential scanning calorimetry was conducted. The plots are shown in the Supporting Information (Figure S2). The exothermic peak, indicative of decomposition of alkyl groups present in the material, has its maximum at 600 °C. A continuous mass loss totaling 10% is observed over the whole temperature range, which is attributed to water desorption as well as removal of alkyl groups.[8] At 300 °C only marginal mass loss of 3% was observed. Thus, it can be concluded that the silylated material is stable under the silylation conditions as well as conditions chosen for hydrothermal stability testing.

**Impact of Silane.** The impact of the amount of silane on the defect healing efficiency was explored using the defect form of B-BEA16 ($BEA16_{def}$). The high concentration of defects in this material is evident from the $^{29}$Si-CP-MAS NMR results (Figure 1). The large Si $Q^3$ peak at −103 ppm associated with

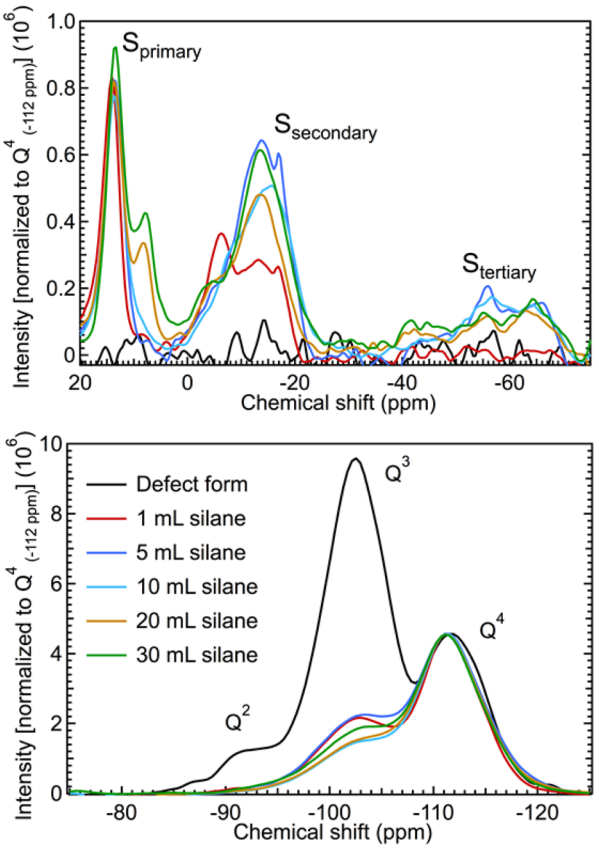


**Figure 1.** $^{29}$Si-CP-MAS NMR spectra of $BEA16_{def}$ with increasing amounts of TMS-Cl (1−20 mL). The intensities are normalized to the $Q^4$ peak intensity at −112 ppm. Primary silylation product ($S_{primary}$) at ∼10−15 ppm, secondary product at about −15 ppm ($S_{secondary}$) and trace amounts of tertiary product ($S_{tertiary}$) at −60 ppm. Color-coding is reported in the legend.

the defect $Si(OH)(OSi)_3$ species significantly outweighs the neighboring $Q^4$ peak (−112 ppm), caused by Si fully surrounded by other Si atoms, $Si(OSi)_4$. Additionally, a peak at −92 ppm was observed, attributed to the $Q^2$ species, $Si(OH)_2(OSi)_2$.[27,28] The appearance of $Q^2$ peaks is related to the presence of silanols in a geminal conformation.[28] Note that the presence of trace amounts of Al (Si/Al 150) results in a signal at −106 ppm,[28] thus causing a slight overestimation of the contribution of defects.

After reaction with TMS-Cl, the $Q^2$ and the $Q^3$ peak intensities decreased significantly. Simultaneously, Si species at higher chemical shifts were observed, which are assigned to primary (∼10−15 ppm) and secondary (about −15 ppm) and tertiary (−60 ppm) silylation products (Scheme 1).[12]

On the basis of the $N_2$-isotherms (Table 2) silylation also led to a decrease in the micropore volume, whereas the mesopore

**Table 2. $N_2$-Physisorption Data for $BEA16_{def}$ Silylated with Increasing Amounts of TMS-Cl**

| sample | BET [$m^2/g$][a] | micropore volume [$cm^3/g$] | mesopore volume [$cm^3/g$] |
|---|---|---|---|
| Defect form | 580 | 0.23 | 0.03 |
| 1 mL silane | 435 | 0.18 | 0.05 |
| 5 mL silane | 340 | 0.14 | 0.05 |
| 10 mL silane | 330 | 0.13 | 0.04 |
| 20 mL silane | 325 | 0.13 | 0.03 |
| 30 mL silane | 330 | 0.13 | 0.04 |

[a]BET: Brunnauer−Emmet−Teller.

volume was hardly affected. As the majority of SiOH groups exists inside the channels, the formation of silylation side products leads to reduced micropore accessibility.[12] There appears to be a maximum accessibility loss. Increasing amounts of silane, beyond 10 mL, hardly reduced the micropore volume. Instead, the mesoporosity appears to be slightly reduced, possibly due to silylation of surface hydroxyls and the generation of a mesoporous structure at the outer surface of the particles. Increasing amounts of TMS-Cl reduced the intensity of the $Q^3$ peak; however, there was no significant difference between 10, 20, and 30 mL of TMS-Cl. Instead, an additional peak (∼10 ppm) is observed at higher silane loadings, which we attribute tentatively to a dimethylchlorosilyl species attached to a defect SiOH. At such large loadings and temperatures, reaction between the methyl group as opposed to the chloro group cannot be ruled out unambiguously leading to the formation of a separate species observed at ∼10 ppm rather than 15 ppm. For further Si−O−Si bridge condensation reactions to occur, yielding tertiary (−60 ppm) and quaternary ($Q^4$) products, three and four silanol groups, respectively, must be within close proximity and correct geometrical orientation to each other.[12] If SiOH groups are solely found on the particle surface, as in case of silica gels, only the formation of primary and secondary products is possible. Therefore, we conclude that the applied postsynthetic treatment method preferentially removed internal SiOH nests.

**Increasing Time on Stream.** Having determined that effective silylation is achieved using as little as 5 mL of silane per 0.75 g of zeolite, it was explored how the time on stream affects the results.

By keeping the sample at 300 °C for extended periods, it can be seen in Figure S7 that the concentration of SiOH groups is slightly reduced. Additionally, more primary and secondary silylation products are converted into tertiary (−60 ppm) and quaternary ($Q^4$) products. The longer interval at 300 °C allows more methyl groups of the deposited silane to react with neighboring SiOH. Thus, the longer the time, the more the microporosity is regained (Table S2).

**Increasing Residence Time.** Adjusting the inlet flow rate of the carrier $N_2$ gas varied the residence time, i.e., the time for a set amount of TMS-Cl to react with the SiOH groups. This neither improved the pore accessibility, nor further decreased


DOI: 10.1021/jacs.5b12785
J. Am. Chem. Soc. 2016, 138, 4408−4415

the defect concentration as monitored by NMR spectroscopy and $N_2$-physisorption (Figure S7 and Table S3). Thus, we conclude that only the longer exposure to high reaction temperatures improves the extent of surface reactions.

**Method Reproducibility.** To demonstrate the general applicability of this approach, $BEA14_{def}$ and $BEA19_{def}$ samples were investigated. Their $^{29}$Si-CP-MAS NMR spectra are shown in Figure 2. An assessment of the $Q^3$ and $Q^2$ signal intensities at

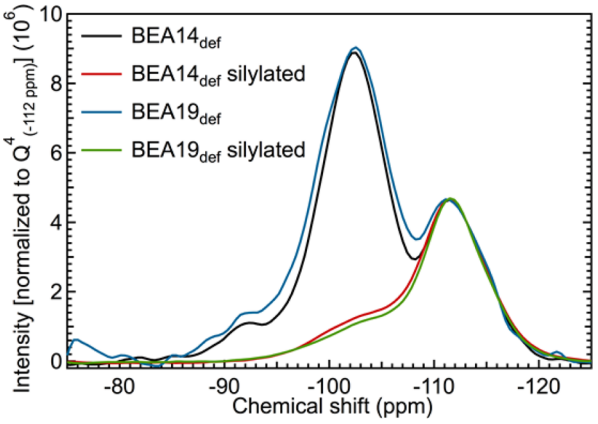


**Figure 2.** Superimposed $^{29}$Si-CP-MAS NMR spectra normalized to intensity of $Q^4$ signal at −112 ppm. The color-coding is reported in the legend.

−103 and −92 ppm, respectively, leads to the conclusion that both materials have a similar extent of defect concentrations. The samples also show a comparable degree of defect removal and loss in pore volume (50−55%; Table 3). The parallel variation in properties of modified and the unmodified materials demonstrate the general applicability of the method.

**Table 3. BEA Samples and Their Porosity upon Silylation and Water Treatment**

| sample | BET [$m^2$/g] | micropore volume [$cm^3$/g] | mesopore volume [$cm^3$/g] |
|---|---|---|---|
| $BEA14_{def}$ | 585 | 0.23 | 0.05 |
| $BEA14_{def}$ + $H_2O$ | 235 | 0.09 | 0.08 |
| $BEA14_{def}$ silylated | 300 | 0.12 | 0.02 |
| $BEA14_{def}$ silylated + $H_2O$ | 255 | 0.1 | 0.18 |
| $BEA19_{def}$ | 620 | 0.25 | 0.08 |
| $BEA19_{def}$ + $H_2O$ | 190 | 0.07 | 0.14 |
| $BEA19_{def}$ silylated | 300 | 0.12 | 0.02 |
| $BEA19_{def}$ silylated + $H_2O$ | 245 | 0.1 | 0.15 |

The IR spectra of the activated materials clearly show the impact of the modification (Figure S3). The overall impact of silylation is best seen in the difference in the IR spectra before and after silylation (Figure 3). The positive peaks indicate increased intensity; the negative peaks illustrate a decrease. The lattice vibration overtones and combination bands between 2090 and 1740 $cm^{-1}$ did not change. In agreement with the $^{29}$Si-CP-MAS NMR spectra, methyl groups remain in the structure (C−H stretching bands at 3000−2800 $cm^{-1}$ and C−H deformation bands at 1410 $cm^{-1}$).[29] Additionally, the bands at 3725 and 3500 $cm^{-1}$ were significantly reduced in both investigated samples. This former band is typically associated with isolated SiOH groups at defect sites and may contain a small contribution of SiOH at external surfaces.[30−34] The latter

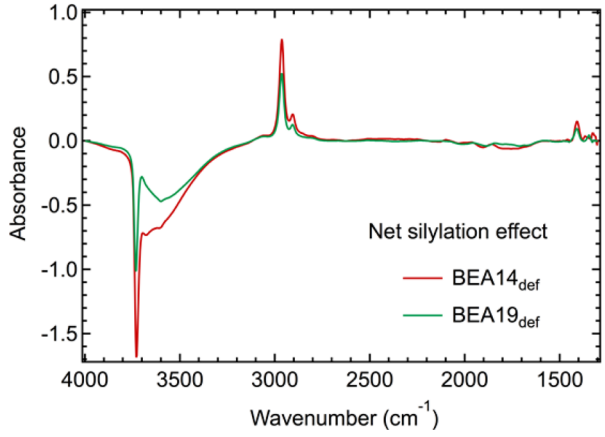


**Figure 3.** Difference IR spectra illustrating the silylation effectiveness for $BEA14_{def}$ and $BEA19_{def}$. Positive peaks indicate generation of vibrations, negative peaks removal of vibrations. The spectra were acquired at 300 °C in vacuum. Color-coding is reported in the legend.

broad band is caused by strong hydrogen bonding of internal SiOH.[23,33−35] The silylation reduced, thus, the intensity of both internal SiOH groups. These had been associated with the framework instability via hydrolysis of adjacent Si−O−Si bonds.[5,7] Protection or removal of these sites is critical to stabilize zeolites kinetically in hot liquid water.

The generation of tertiary silylation products, the extensive reduction in $Q^3$ peak intensities, and the decreased intensities of bands associated with internal SiOH groups show conclusively that the extensive removal of internal structural defects stabilizes. These findings are in agreement with Resasco et al. noting that short-chain alkylchlorosilanes were more effective than long-chain ones to stabilize zeolites in hot liquid water.[9]

**Hydrothermal Stability of Modified Zeolites.** The impact of removing the internal SiOH of $BEA14_{def}$ and $BEA19_{def}$ on the stability in hot liquid water was explored in an autoclave at 160 °C for 48 h in an excess of water (1:200). These conditions lead to hydrolysis of the siloxane bonds in the zeolite framework and partial dissolution of the crystal and potential reprecipitation of $SiO_2$.[5,6]

The relative crystallinity of the parent and silylated zeolite samples after hydrothermal treatment was estimated by analyzing the areas under all peaks in the X-ray diffractograms allowing to quantitatively assess the effect of stabilization. The stacking faults in the BEA framework lead to sharp and broad peaks in the X-ray diffractograms, with the two main peaks appearing at $\sim 2\theta = 7.5°$ and $2\theta = 22°$.[14] In polymorph B (BEB), these reflections are associated mainly with (−111), (110) and (−332), (330) planes, respectively, while in polymorph A (BEA), planes (101) and (302) have the strongest signal intensity.[15] A substantial loss in the intensity of the XRD peaks, e.g., as observed for $2\theta = 7.5°$ in Figure 4, in the course of framework hydrolysis is attributed to the long-range order of the individual crystallites being reduced.

Previous work associated this intensity loss with the removal of atoms and generation of defects disrupting the coherency of the related lattice planes.[5] The fact that only certain planes, in this case mainly (101) for BEA and (−111), (110) in BEB, are affected, helps to deduce the degradation mechanism.[5] These planes run parallel to 4- and 6-membered rings and dissect the same T-O-T bridges ($T_1$-O-$T_1$, $T_1$-O-$T_2$ and $T_2$-O-$T_2$) in the pristine zeolite.


DOI: 10.1021/jacs.5b12785
J. Am. Chem. Soc. 2016, 138, 4408−4415

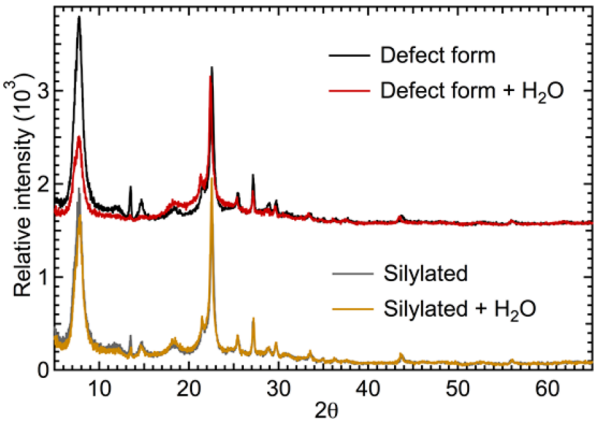


**Figure 4.** Impact of zeolite hydrothermal treatment on the crystallinity of the BEA framework is shown on the example of XRD patterns collected for the parent and treated $BEA14_{def}$. The color-coding is reported in the legend.

While the defect form lost about 20% of its crystallinity after water treatment at 160 °C for 48 h, the silylated material remained almost unchanged (Figure 4). A slight shift in the peak position was observed for the parent water-treated material, indicating the modification of the unit cell lattice parameters induced by the degradation of the zeolite. Similar observations were made for $BEA19_{def}$ (see Figure S6). The generation of a separate phase was observed for the water-treated parent material, which is tentatively attributed to magadiite, a layered silicate.[36,37] The silylated material, in contrast, did not form a new phase, signifying the stabilization.

Framework hydrolysis led to the formation of mesoporosity as well as to partial destruction of the microporous character of the unmodified sample (Table 3), in addition to the loss of crystallinity (as seen by XRD). Yet, the silylated material hardly changed its microporosity after exposure to hot liquid water.

$N_2$ sorption isotherms in Figure 5 show two different hysteresis shapes. Water treatment of the stabilized material

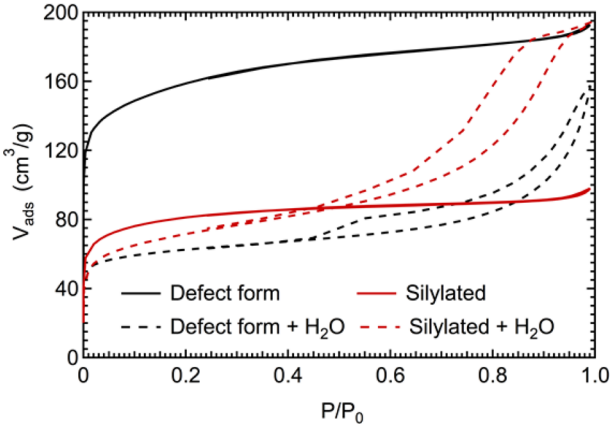


**Figure 5.** $N_2$-sorption isotherms for the parent and silylated form of $BEA14_{def}$ and their respective water-treated counterparts are shown. The color-coding is reported in the legend.

leads to the formation of a hysteresis loop resembling H2 type,[38] indicating nonuniform cylindrical pore shapes. The pores are likely to have ink-bottle shapes due to a longer retention of the adsorbate at high relative pressures during the desorption process. This specific type has a smaller pore mouth than pore body, hence, the nonuniform hysteresis shape.[39] For the unmodified material, water treatment leads to a very different and atypical hysteresis.

While only the isotherm of $BEA14_{def}$ is presented here, $BEA19_{def}$ behaves the same (see Figure S5). We hypothesize, therefore, that introduction of water to the silylated material at elevated temperatures leads to ink-bottle mesopores, whereas the unmodified material forms ill-defined mesopores or mesovoids. The differences in the mesopore shapes are a direct effect of the silylation.

Having established that water treatment of the silylated material does not only result in retention of crystallinity and microporosity, but also changes the mesoporosity compared to the unmodified material, we turn to transmission electron microscopy (TEM). The images in Figure 6 show different

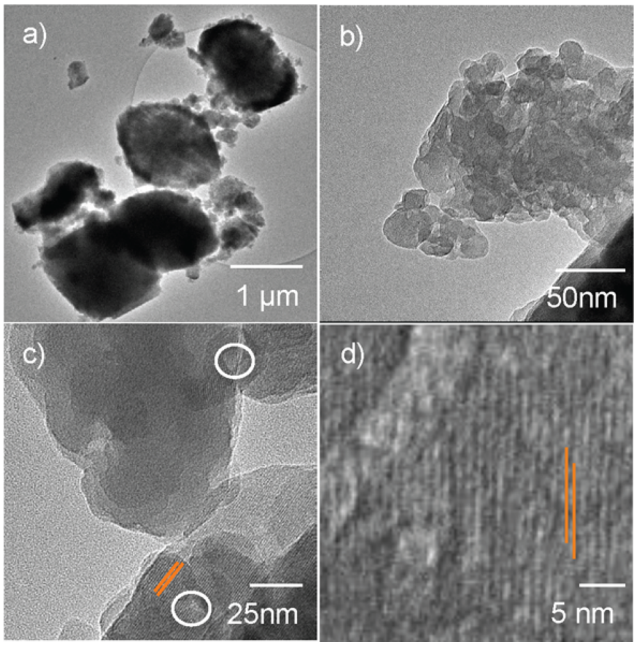


**Figure 6.** TEM images of water treated defect form, $BEA14_{def}$ + $H_2O$. Mesopores are shown with white circles, lattice fringes in orange. The fringes are still present on observed small particles.

magnifications of the defect form $BEA14_{def}$ after water treatment. The dark areas are attributed to increasing sample thickness. Small crystallites adjacent to larger particles are observed. The presence of lattice fringes indicates that these fragments are crystalline.

The small particles are agglomerates of even smaller crystallites, forming intercrystal mesovoids among them, in line with the hysteresis shape observed with $N_2$ sorption reported above. This reduction in particle size is attributed to the cleavage of siloxy bonds and the subsequent dissolution of silica leading to cracking and fracturing of the crystals.[5] TEM images in Figure 7 illustrate the macroscopic morphology of silylated particles and their porous character after water treatment. The significant difference between water-treated defective and silylated material is the absence of small crystallites in the latter. Water-treatment has no effect on the macroscopic morphology of the stabilized materials, as can be seen by comparison with TEM images in Figure S9 of the Supporting Information. However, mesopores are observed, as micropores remained clearly visible. While the mesoporosity is


DOI: 10.1021/jacs.5b12785
J. Am. Chem. Soc. 2016, 138, 4408−4415

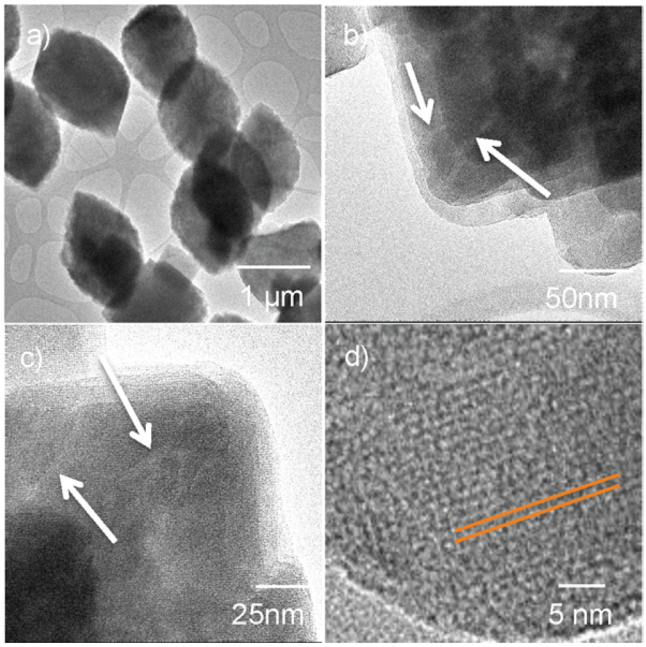


**Figure 7.** TEM images of water-treated silylated material, $BEA14_{def}$ silylated + $H_2O$. Channel-type mesopores can be observed next to white arrows, lattice fringes in orange. No fractured particles were observed.

similar, the shape of the pores formed is different between the defect and the stabilized material. Long elongated mesopores are observed at the edges of the water-treated silylated material.

Similar observations were made for $BEA19_{def}$, with the images shown in the Supporting Information (Figure S10). However, that material showed less fracturing than $BEA14_{def}$. Both the unmodified and silylated material appear quite similar after water-treatment in terms of particle morphology and size. However, at closer inspection, the unmodified material presents a lower particle density due to excessive formation of mesopores.

We conclude that silylation removes most defects resulting in a drastic retardation of the framework hydrolysis. The mesoporosity generated is presented in the form of channels with narrow pore mouths due to the fact that cleavage of the Si−O−Si bonds progresses along the few remaining defects. In the parent defective form, hydrolysis proceeds at more sites and distributed throughout the crystal, leading to fragmentation of crystallites.

The XRD results confirm that crystallinity is retained in the stabilized material after water treatment, inferring that fewer atoms are removed such that the coherency of the planes is less disrupted. In the defect form on the other hand, the reduction in crystallite size, as well as extensive removal of atoms spread over the whole particle, leads to a disruption of the plane integrity and resulting loss in XRD peak intensity.

The XRD and TEM analyses agree well with the $^{29}$Si-CP-MAS NMR analysis (Figure 8) that shows the comparison of the SiOH intensities measured for the parent and stabilized zeolite $BEA14_{def}$ upon treatment in hot liquid water (for $BEA19_{def}$ see Figure S8). The $Q^3$ signal intensity was significantly reduced for the water-treated unmodified material. We attribute the loss in $Q^3$ signal intensity to fracturing and loss of microporosity. The starting material has a high fraction of internal SiOH giving rise to a large $Q^3$ signal (−103 ppm).

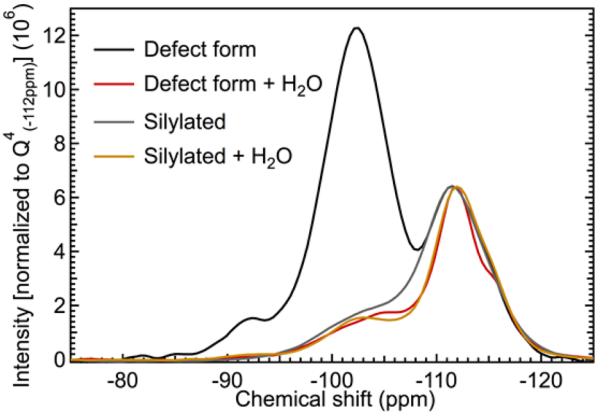


**Figure 8.** $^{29}$Si-CP-MAS NMR spectra of unmodified and silylated $BEA14_{def}$ before and after water treatment at 160 °C for 48 h. Color-coding is reported in the legend. The full spectrum can be found in the Supporting Information (Figure S8).

Water treatment removes a major fraction of these silanols as it cleaves neighboring Si−O−Si bridges, leading to fracturing. The small crystallites still yield a $Q^4$ signal.

However, due to the particles being mostly defect free, the $Q^3$ signal is significantly reduced, with the remaining signal being contributed to surface SiOH groups (−100 ppm).[40] It is noted in passing that the cross-polarization enhancement factor varies between internal silanols and surface silanols hindering a quantitative assessment of SiOH concentrations.[40,41]

In the case of the stabilized material, only small changes were observed by $^{29}$Si-CP-MAS NMR spectroscopy, which is in agreement with minor changes in crystallinity (XRD) and morphology (TEM). The formation of mesopores at the expense of micropores leads to the removal of material from the crystal body. This material initially contained a relatively high concentration of SiOH groups in the form of nests ($Q^3$). The conditions of the cross-polarization experiment were optimized to enhance these SiOH nests with a high density of protons (−103 ppm). However, the resulting mesopores have mostly surface SiOH groups (−100 ppm) on the walls. They are isolated and the lower proton concentration is likely to result in a lesser enhancement and thus a smaller peak in the $Q^3$ region.

## ■ CONCLUSIONS

The zeolite postsynthetic silylation treatment is demonstrated to significantly improve material stability in hot liquid water, under retention of crystallinity and microporosity. Silylation reduces efficiently the concentration of internal structural defects, known to be the primary active sites for framework hydrolysis. The reported procedure is expected to be applicable to a range of zeolites prone to hydrolysis. The silylation treatment is suggested as a potential pathway toward stabilizing and extending the lifetime of Al-rich zeolites enhancing their use as a solid acid catalyst in aqueous phase, e.g., dehydration of alcohols and alkylation of phenols in hot liquid water.

## ■ EXPERIMENTAL SECTION

**Chemicals.** The silylating agent, trimethylchlorosilane (TMS-Cl > 99.0%), was obtained from Sigma-Aldrich and used as received.

**H-Form.** The boron zeolites were synthesized according to the procedure reported by Derewinski et al.[19] and calcined at 550 °C for 6 h in air to remove the template. The calcined Na-form was ion-exchanged with 0.1 M $NH_4NO_3$ solution for 2 h at 80 °C under stirring conditions. The suspension was then centrifuged, the solid


DOI: 10.1021/jacs.5b12785
J. Am. Chem. Soc. 2016, 138, 4408−4415

redispersed in $NH_4^+$ solution, and the procedure repeated two more times. Upon completion, the material was dried at 80 °C overnight, before calcining it once more at 450 °C for 6 h in air to yield the H-form.

**Defect Form.** The defect form was generated by washing the H-form of the desired zeolite for 2 h at 50 °C with Milli-Q water (1 g/50 mL $H_2O$). The suspension was then centrifuged, and the solid residue was washed once more under the same conditions. This was followed by another centrifugation step and drying overnight. It yielded the defective starting material used for the following silylation step.

**Silylation.** The silylation procedure was adapted from a previously described procedure, designed for silica gels and silicalite in closed ampules.[12,26] In our case, an open system with flow characteristics was designed.

The sample, defect form, was suspended within a quartz tube and placed in a tube furnace. The quartz tube was then connected via Teflon tubing to a saturator containing the silylating agent cooled with an ice bath. $N_2$ carrier gas, set to a specific flow rate, enabled the transport of silane vapors to the reactor and subsequent removal of defects. The other end of the quartz tube was connected to an oil bubbler. If desired, the flow of $N_2$ could be shut off, essentially generating a reactive atmosphere saturated with silane vapors.

A typical silylation reaction consisted of an activation period, during which the sample was heated, under the flow of $N_2$, to the desired reaction temperature, typically 300 °C, within 1 h and then kept at this temperature for 2 h. Then, the gas stream was passed through a saturator filled with the silane and allowed to react with the sample. Specific reaction parameters are reported in the Supporting Information. The silylated samples were subsequently removed from the quartz tube and used without further purification.

**Stability Testing.** Zeolites underwent hydrothermal water treatment in Teflon lined batch autoclaves at 160 °C. Typically, 300 mg of zeolite and 60 mL of deionized Milli-Q water (1:200) were added to an autoclave, which was then placed in an oven at 160 °C. The autoclave was rotated inside the oven. The reactor was kept under these conditions for 48 h before cooling it to room temperature, centrifuging the suspension, and drying the solid residue at 80 °C overnight.

**Characterization Methods.** *X-ray Diffraction (XRD).* XRD patterns were collected on a Rigaku Mini Flex II benchtop X-ray diffractometer using a Cu K$\alpha$ radiation of 0.154056 nm (30 kV and 15 mA). Experiments were conducted on a rotating powder sample holder in a $2\theta$ range of 5−60° with a step size of 0.02°/s. All measurements were performed under ambient conditions.

*$^{29}$Si-MAS NMR.* The cross-polarization (CP) $^{29}$Si-MAS NMR experiments were performed using a Varian Inova 89-mm wide-bore 300 MHz NMR spectrometer and a 5 mm HXY MAS Chemagnetics style probe. The following parameters for the cross-polarization pulse sequence were used: the H90 was set to 4 $\mu$s, the contact time was 3 ms, and the decoupling field of 62.5 kHz was applied for 10 ms during the acquisition time. The spinning speed was set to 5 kHz.

*Helium Ion Microscopy (HIM).* HIM images were obtained using 35 keV He ions with 0.1 pA beam current at normal incidence. Secondary electrons were detected using an Everhart−Thornley detector. For HIM imaging, a very thin layer of carbon (<1 nm) was coated using a carbon sputter deposition system as the samples were completely insulated. The instrument resolution was 0.35 nm.

*Thermogravimetric Analysis (TGA).* A Netzsch STA 449C Jupiter system with an integrated differential scanning calorimeter (DSC) was used to analyze thermal stability. A heating ramp of 5 °C/min up to 1000 °C under a flow of 50 mL/min synthetic air and 15 mL/min $N_2$ was chosen. Typically, 20 mg of material was tested in an $Al_2O_3$ crucible. The curves were corrected against an empty reference crucible.

*Transmission Electron Microscopy (TEM).* Imaging was performed on am FEI Tecnai F20 instrument, operated at 200 keV. The images were collected in TEM mode. The samples were prepared by gently crushing the powder between two glass slides, and rubbing a holey carbon grid across the slide with one drop of ethanol.

*$N_2$-Physisorption.* The BET surface areas and pore size distributions were obtained by physisorption in a Micromeritics ASAP 2020 unit. The pore volumes were determined using the Horvath−Kawazoe method.[42] Micromeritics analysis software provided the method.

*Infrared (IR) Spectroscopy.* The samples for IR measurements were prepared as self-supporting wafers with a density of approximately 10 mg/cm$^2$. Upon loading in the IR-cell, the samples were evacuated to $1.0 \times 10^{-7}$ mbar and heated in intervals to 150 and 300 °C and kept at 300 °C for 12 h. The heating rate is set to 20 °C/min. Infrared spectra are recorded on a ThermoScientific Nicolete FTIR spectrometer using a MCTA detector with a resolution of 4 cm$^{-1}$. A total of 128 scans were accumulated for each spectrum. The spectra are normalized to the overtones and combination vibrations of the BEA lattice between 2090 and 1740 cm$^{-1}$.[43]

## ■ ASSOCIATED CONTENT

### Supporting Information

The Supporting Information is available free of charge on the ACS Publications website at DOI: 10.1021/jacs.5b12785.

XRD patterns, $N_2$ sorption isotherms, TGA/DSC curves, HIM and TEM images, IR and NMR spectra (PDF)

## ■ AUTHOR INFORMATION


### Corresponding Authors

*miroslaw.derewinski@pnnl.com

*Johannes.Lercher@pnnl.gov


### Notes

The authors declare no competing financial interest.

## ■ ACKNOWLEDGMENTS

The authors would like to thank B. W. Arey (PNNL) for HIM measurements, J. L. Fulton and D. M. Camaioni for their valuable input and discussion. A.V., S.D.B., I.A., and J.A.L. were supported by the U.S. Department of Energy, Office of Science, Office of Basic Energy Sciences. Pacific Northwest National Laboratory (PNNL) is a multiprogram national laboratory operated for DOE by Battelle. S.P. and M.A.D. acknowledge support by the Materials Synthesis and Simulation Across Scales (MS$^3$ Initiative) conducted under Laboratory Directed Research & Development Program at PNNL.

## ■ REFERENCES


(1) Yilmaz, B.; Müller, U. *Top. Catal.* **2009**, *52*, 888−895.

(2) Zhao, C.; Kou, Y.; Lemonidou, A. A.; Li, X.; Lercher, J. A. *Chem. Commun.* **2010**, *46*, 412−414.

(3) Zhao, C.; Camaioni, D. M.; Lercher, J. A. *J. Catal.* **2012**, *288*, 92−103.

(4) Ravenelle, R. M.; Schüßler, F.; D'Amico, A.; Danilina, N.; van Bokhoven, J. A.; Lercher, J. A.; Jones, C. W.; Sievers, C. *J. Phys. Chem. C* **2010**, *114*, 19582−19595.

(5) Vjunov, A.; Fulton, J. L.; Camaioni, D. M.; Hu, J. Z.; Burton, S. D.; Arslan, I.; Lercher, J. A. *Chem. Mater.* **2015**, *27*, 3533−3545.

(6) Vjunov, A.; Derewinski, M. A.; Fulton, J. L.; Camaioni, D. M.; Lercher, J. A. *J. Am. Chem. Soc.* **2015**, *137*, 10374−10382.

(7) Zhang, L.; Chen, K.; Chen, B.; White, J. L.; Resasco, D. E. *J. Am. Chem. Soc.* **2015**, *137*, 11810−11819.

(8) Zapata, P. A.; Faria, J.; Ruiz, M. P.; Jentoft, R. E.; Resasco, D. E. *J. Am. Chem. Soc.* **2012**, *134*, 8570−8578.

(9) Zapata, P. A.; Huang, Y.; Gonzalez-Borja, M. A.; Resasco, D. E. *J. Catal.* **2013**, *308*, 82−97.

(10) Huang, M.; Adnot, A.; Kaliaguine, S. *J. Chem. Soc., Faraday Trans.* **1993**, *89*, 4231−4237.

(11) Klinowski, J.; Thomas, J. M.; Anderson, M. W.; Fyfe, C. A.; Gobbi, G. C. *Zeolites* **1983**, *3*, 5−7.




DOI: 10.1021/jacs.5b12785
*J. Am. Chem. Soc.* 2016, 138, 4408−4415

(12) Kraushaar, B.; Van De Ven, L. J. M.; De Haan, J. W.; Van Hooff, J. H. C. *Stud. Surf. Sci. Catal.* **1988**, *37*, 167−174.
(13) Kraushaar, B.; de Haan, J. W.; van De Ven, L. J. M.; van Hooff, J. H. C. *Z. Anorg. Allg. Chem.* **1988**, *564*, 72−80.
(14) Higgins, J. B.; LaPierre, R. B.; Schlenker, J. L.; Rohrman, A. C.; Wood, J. D.; Kerr, G. T.; Rohrbaugh, W. J. *Zeolites* **1988**, *8*, 446−452.
(15) Baerlocher, C.; McCusker, L. B. *Database of Zeolite Structures*. http://www.iza-structure.org/databases/ (accessed October 2015).
(16) Newsam, J. M.; Treacy, M. M. J.; Koetsier, W. T.; Gruyter, C. B. D. *Proc. R. Soc. London, Ser. A* **1988**, *420*, 375−405.
(17) Reddy, K. S. N.; Eapen, M. J.; Joshi, P. N.; Mirajkar, S. P.; Shiralkar, V. P. *J. Inclusion Phenom. Mol. Recognit. Chem.* **1994**, *20*, 197−210.
(18) de Ruite, R.; Famine, K.; Kentgens, A. P. M.; Jansen, J. C.; van Bekkum, H. *Zeolites* **1993**, *13*, 611−621.
(19) Derewinski, M.; Renzo, F. D.; Espiau, P.; Fajula, F.; Nicolle, M.-A. *Stud. Surf. Sci. Catal.* **1991**, *69*, 127−134.
(20) Kerr, G. T. *J. Phys. Chem.* **1969**, *73*, 2780−2782.
(21) Kuehl, G. H., U.S. Patent 4 661 467, 1987.
(22) Fild, C.; Shantz, D. F.; Lobo, R. F.; Koller, H. *Phys. Chem. Chem. Phys.* **2000**, *2*, 3091−3098.
(23) de Ruiter, R.; Kentgens, A. P. M.; Grootendorst, J.; Jansen, J. C.; van Bekkum, H. *Zeolites* **1993**, *13*, 128−138.
(24) de Ruiter, R.; Jansen, J. C.; van Bekkum, H. *Zeolites* **1992**, *12*, 56−62.
(25) Cundy, C. S.; Cox, P. A. *Chem. Rev.* **2003**, *103*, 663−702.
(26) Rutten, G.; van de Ven, A.; de Haan, J.; van de Ven, L.; Rijks, J. *J. High Resolut. Chromatogr.* **1984**, *7*, 607−614.
(27) Fyfe, C. A.; Gobbi, G. C.; Kennedy, G. J. *J. Phys. Chem.* **1985**, *89*, 277−281.
(28) Hunger, M.; Karger, J.; Pfeifer, H.; Caro, J.; Zibrowius, B.; Bulow, M.; Mostowicz, R. *J. Chem. Soc., Faraday Trans. 1* **1987**, *83*, 3459−3468.
(29) Mirth, G.; Lercher, J. A.; Anderson, M. W.; Klinowski, J. *J. Chem. Soc., Faraday Trans.* **1990**, *86*, 3039−3044.
(30) Woolery, G. L.; Alemany, L. B.; Dessau, R. M.; Chester, A. W. *Zeolites* **1986**, *6*, 14−16.
(31) Datka, J.; Tużnik, E. *Zeolites* **1985**, *5*, 230−232.
(32) Maier, S. M.; Jentys, A.; Lercher, J. A. *J. Phys. Chem. C* **2011**, *115*, 8005−8013.
(33) Takei, T.; Kato, K.; Meguro, A.; Chikazawa, M. *Colloids Surf., A* **1999**, *150*, 77−84.
(34) Krijnen, S.; Harmsen, R. J.; Abbenhuis, H. C. L.; Van Hooff, J. H. C.; Van Santen, R. A. *Chem. Commun.* **1999**, 501−502.
(35) Holm, M. S.; Svelle, S.; Joensen, F.; Beato, P.; Christensen, C. H.; Bordiga, S.; Bjørgen, M. *Appl. Catal., A* **2009**, *356*, 23−30.
(36) Fletcher, R. A.; Bibby, D. M. *Clays Clay Miner.* **1987**, *35*, 318−320.
(37) Eugster, H. P. *Science* **1967**, *157*, 1177−1180.
(38) Sing, K. S. W.; Everett, D. H.; Haul, R. A. W.; Moscou, L.; Pierotti, R. A.; Rouquerol, J.; Siemieniewska, T. *Pure Appl. Chem.* **1985**, *57*, 603−619.
(39) Leofanti, G.; Padovan, M.; Tozzola, G.; Venturelli, B. *Catal. Today* **1998**, *41*, 207−219.
(40) Engelhardt, G.; Lohse, U.; Samoson, A.; Mägi, M.; Tarmak, M.; Lippmaa, E. *Zeolites* **1982**, *2*, 59−62.
(41) Sindorf, D. W.; Maciel, G. E. *J. Phys. Chem.* **1982**, *86*, 5208−5219.
(42) Horváth, G.; Kawazoe, K. *J. Chem. Eng. Jpn.* **1983**, *16*, 470−475.
(43) Jentys, A.; Lercher, J. A. *Stud. Surf. Sci. Catal.* **1989**, *46*, 585−594.



DOI: 10.1021/jacs.5b12785
*J. Am. Chem. Soc.* 2016, 138, 4408−4415